IEEE Access
Multidisciplinary | Rapid Review | Open Access Journal

Received November 8, 2019, accepted November 21, 2019, date of publication November 25, 2019,
date of current version December 11, 2019.

Digital Object Identifier 10.1109/ACCESS.2019.2955714

Phase-Shifted Carrier Pulse-Width Modulation Algorithm With Improved Dynamic Performance for Modular Multilevel Converters

MINH HOANG NGUYEN[1], SANGSHIN KWAK[1], (Member, IEEE), AND TAEHYUNG KIM[2], (Senior Member, IEEE)

[1]School of Electrical and Electronics Engineering, Chung-Ang University, Seoul 06974, South Korea
[2]Department of Electrical and Computer Engineering, University of Michigan–Dearborn, Dearborn, MI 48128, USA

Corresponding author: Sangshin Kwak (sskwak@cau.ac.kr)

This work was supported by the National Research Foundation of Korea (NRF) grant funded by the Korea Government (MSIP) (NRF-2017R1A2B4011444).

ABSTRACT High modularity, easy scalability, and superior harmonic performance, comprising the topology with the most potential for medium- to high-voltage high-power applications, are representative features of a modular multilevel converter (MMC). Each application of a MMC requires a proper scheme such that it conforms to control objectives such as correct submodule capacitor voltage balancing control and the suppression of circulating current. Over the past few years, various studies have been presented that meet the MMC requirements through both classical control-based pulse-width modulation and model predictive control, although some drawbacks exist for both control concepts. The dynamic performance of the classical control methods with proportional-integral or proportional-resonant controllers is unsatisfactory, and the requirement of proportional-integral parameters tuning procedure makes converter operation performance depends on proportional-integral parameters adjustment. Meanwhile, model predictive control performance depends significantly on the mathematical model of a system, and weighting factor selection is tedious. In this paper, we propose an improved phase-shifted carrier pulse-width modulation method and capacitor voltage balancing control that inherits the merits from both classical control and model predictive control. Meanwhile, the proposed control method eliminates the requirement of the tedious proportional-integral parameters tuning procedure and improves the dynamic performance compared with the conventional phase-shifted carrier pulse-width modulation-based proportional-integral controller method. Simulations and experiments were conducted to demonstrate the proposed method's properness.

INDEX TERMS Modular multilevel converter, phase-shifted carrier pulse-width modulation, submodule capacitor voltage balancing control.

I. INTRODUCTION

In recent years, there has been a growing trend toward using multilevel converters in the industry. Various multilevel converter topologies have been developed over past decades, although few have received wide acceptance for use in industry. It should be mentioned that among the various multilevel converter topologies, the three-level neutral point clamped converter (3L-NPC) [1], flying capacitor converter (FC) [2], and cascaded H-bridge (CHB) converter [3] have been most closely studied. However, there are problems with these multilevel topologies. In terms of high-power and high-voltage applications, the 3L-NPC and FC topologies require a dramatic increase in the number of clamping diodes or FCs, which leads to high complexity in controlling the capacitor voltage [1], [4], [5]. Meanwhile, the CHB topology has a modular structure and still requires a great many of isolated DC sources, which increases the cost of the whole converter system. To address such challenges, the modular multilevel converter (MMC), first presented by Lesnicar and Marquardt in 2003 [6], has gained much attention in terms of the demand for medium- to high-power applications. Compared with other multilevel converter topologies, the modular and scalable characteristics of MMC allow it to generate any

The associate editor coordinating the review of this manuscript and approving it for publication was Huiqing Wen.

voltage level. Furthermore, the cascaded submodules (SMs) configuration means that the MMC can provide excellent quality output current and output voltage without requiring filters [7].

In spite of the benefits of MMC, a proper control scheme is indispensable to achieve several objectives such as proper magnitude and frequency of AC output currents, minimization of the circulating current, and balance of the SM capacitor voltages. Thus far, classical control methods and model predictive control (MPC) methods have been used to meet the MMC control objectives. In classical control methods, proportional-integral (PI) [8] and proportional-resonant (PR) [9] controllers have been used individually to control each objective. Meanwhile, a pulse-width modulator is necessary to generate the gating signals for SMs. In [8], Hagiwara and Akagi introduce a representative control concept among classical control methods, an approach which controls each SM of the MMC independently. The balance of SM capacitor voltages is managed by an averaging control and a balancing control which control the average SM capacitor voltage in each phase-leg and individual SM capacitor voltage, respectively. Subsequently, their output levels are added to each SM reference modulating signal. Furthermore, the SM capacitor voltage balancing task can be carried out using a control action term that is added to the upper and subtracted from the lower arm modulation index [10]. In [10], the voltage error between the average upper and average lower arm voltages through a linear PI controller is multiplied by the circulating current to generate the control action term. In classical control methods, the dominant second-order harmonic and higher-order harmonics of the circulating current can be suppressed using a synchronous reference frame with linear controllers [11]. Besides, various resonant and repetitive controllers have been used to eliminate the second-order harmonic and higher-order harmonics in a similar manner to that presented in [12]–[15]. Capacitor voltage balancing control and circulating current control are mostly used to work with various PWM methods, such as phase-shifted carrier PWM (PSC-PWM) [8] and level-shifted carrier PWM (LSC-PWM) which are classified as phase-disposition PWM (PD-PWM) [16], phase-opposition disposition PWM (POD-PWM), or alternate POD-PWM (APOD-PWM) [17]. Among these, PD-PWM and PSC-PWM are widely utilized due to the lowest line-to-line harmonic voltage distortion and the highest equivalent switching frequency, respectively. However, the uneven switching state distribution of PD-PWM negatively impacts the harmonic distortion of the output voltage and induces a large magnitude circulating current. To address this drawback, PSC-PWM, which is the most commonly used method in the CHB converter [18], is much preferred for MMC.

Even though the classical control method offers simple and easy implementation, the performance of this control scheme depends on the design of the controller parameters. Due to the highly nonlinear with a wide range of operational points and the utilization of various closed loops, the dynamic performance of the MMC system with PI or PR controller is unsatisfactory [19]–[21]. Additionally, a proper tuning procedure for the PI parameters is indispensable.

Unlike the classical control method, MPC does not need both modulator and PI or PR controllers because the switching states are generated directly [20]. Furthermore, MPC allows the simultaneous control of multiple objectives with a cost function. Eliminating the PI controllers significantly improves the MMC's dynamic performance [21]. MPC has gained much attention in multilevel control due to its distinctive advantages, but there is a drawback: the conventional MPC known as the finite control set MPC (FCS-MPC) has to deal with the significant increase in available switching states that corresponds to the number of SMs, which increases the MPC method's complexity and calculation burden. Several research groups have proposed control schemes to reduce the calculation burden of the MPC method [22]–[25], although the dynamic performance is lowered [22]. Additionally, the MPC method's performance is dependent on the system's mathematical model and the selection of weighting factors in the cost function. The weighting factors selection procedure in the MPC method is identical to the parameter tuning procedure in terms of the tedium when selecting the optimal value while simultaneously maintaining proper control of the objectives.

In terms of medium-voltage applications, an MMC with few SMs is feasible, and a high switching frequency is needed to achieve high-quality output voltage [26], [27]. Herein, we propose an improved PSC-PWM method and a new capacitor voltage balancing control scheme for controlling MMC where regulating the AC output current and circulating current has been implemented with their predicted values substituted for reference ones. Subsequently, the optimal upper and lower arm reference modulating signals can be generated based on the relationship between the arm voltage, the AC output current, and the circulating current. Meanwhile, the capacitor voltage balancing control is employed by rescaling the modulation indexes of each associated modulation signal among the SMs. The relationship between the arm current and the magnitude of the capacitor voltage is evaluated to calculate a coefficient, which is assigned to the corresponding SM modulation signal to rescale its modulation index. As a whole, the proposed method has the following advantages: 1) no requirement for PI controllers to achieve objectives, which allows avoiding the PI parameters tuning procedure and dependence of operation performance on PI parameters adjustment; 2) improved dynamic performance of the PSC-PWM method compared with conventional PSC-PWM-based PI controllers; 3) achieving capacitor voltage balancing control in a closed-loop manner; and 4) avoiding unwanted switching actions. The proposed method's performance was verified with simulation and experimental studies.

This paper is organized as follows: Section II contains a description of the basic structure of the MMC and a review of conventional PSC-PWM-based PI controllers [8].

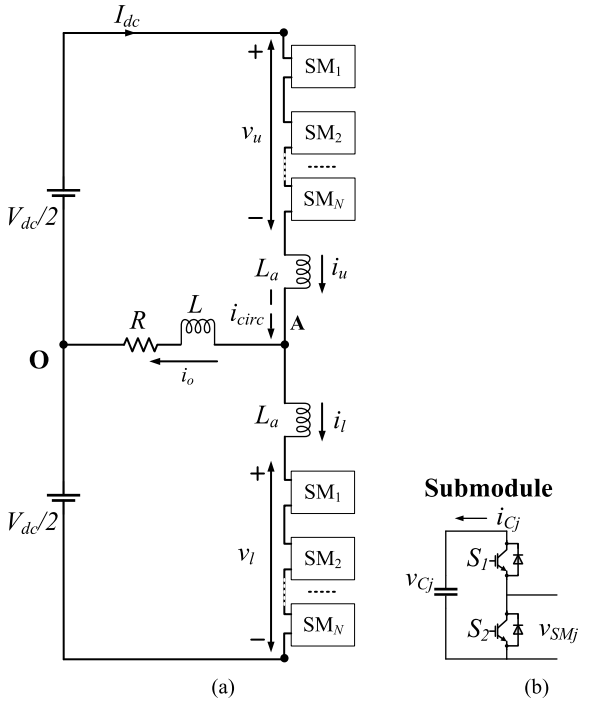

FIGURE 1. A circuit diagram of a single phase MMC: (a) the phase of the MMC and (b) the half-bridge submodule. The upper (lower) arm is represented by a subscript "*u*" ("*l*"). Each arm comprises *N* SMs which are connected in series with an inductor L_a used to limit the arm current.

TABLE 1. Output voltage of SM.

SM state	S_1	S_2	v_{SM}
Inserted	On	Off	v_C
Bypassed	Off	On	0

Section III presents the proposed method in detail. The proposed method's validity verified via simulated and experimental studies on a single-phase MMC prototype is reported in Section IV. Finally, Section V contains conclusions of the study.

II. MMC TOPOLOGY AND CONVENTIONAL PSC-PWM CONTROL

A. MMC TOPOLOGY

Figure 1 illustrates a typical configuration of a one-phase MMC consisting of two arms. In terms of SM, the half-bridge topology in Figure 1(b) among several SM topologies such as half-bridge, full-bridge, and multilevel flying capacitor SMs is implemented in this investigation due to its simplicity and low power loss characteristics [7], [28]. The half-bridge SM can generate only zero and positive voltages which correspond to the switching states of switches S_1 and S_2, as reported in Table 1.

In Figure 1, the mathematical model of MMC can be generated by applying Kirchhoff's current law [7], [28], the AC output current i_o and the circulating current i_{circ} equations

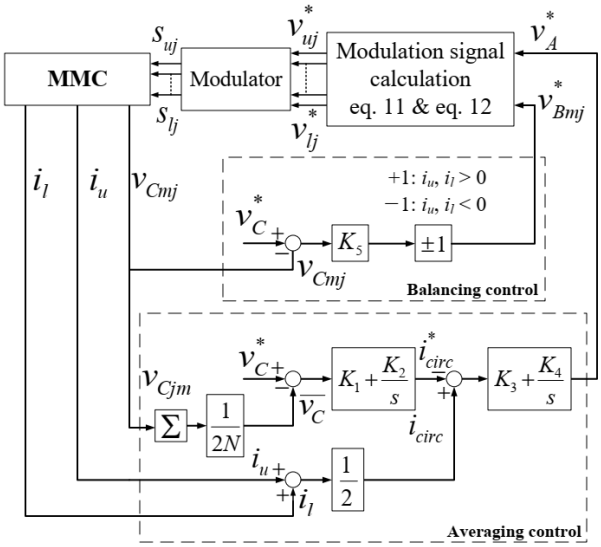

FIGURE 2. The structure of the conventional PSC-PWM control scheme based PI controllers.

can be expressed as

$$i_o = i_u - i_l, \tag{1}$$

$$i_{circ} = \frac{1}{2}\left(i_u + i_l\right), \tag{2}$$

where i_u and i_l are the upper arm current and lower arm current, respectively. The voltage relationship of MMC in Figure 1 by means of Kirchhoff's voltage law can be described as

$$\frac{V_{dc}}{2} - v_u - L_a\frac{di_u(t)}{dt} - Ri_o - L\frac{di_o(t)}{dt} = 0, \tag{3}$$

$$-\frac{V_{dc}}{2} + v_l + L_a\frac{di_l(t)}{dt} - Ri_o - L\frac{di_o(t)}{dt} = 0, \tag{4}$$

where v_u and v_l represent the upper arm voltage and lower arm voltage, respectively.

Adding (3) and (4) and substituting for i_o from (1), the mathematical dynamic of the AC output current is given by

$$\frac{di_o(t)}{dt} = \left(\frac{1}{2L + L_a}\right)\left[v_l(t) - v_u(t) - 2Ri_o(t)\right]. \tag{5}$$

In the same manner, the mathematical dynamic of the circulating current can be deduced by subtracting (3) from (4) and substituting for i_{circ} from (2):

$$\frac{di_{circ}(t)}{dt} = \left(\frac{1}{2L_a}\right)\left[V_{dc} - v_u(t) - v_l(t)\right]. \tag{6}$$

Equations (1) – (4) contribute toward a generalized dynamic model of the MMC which can be used for the control objectives.

B. CONVENTIONAL PSC-PWM CONTROL

Figure 2 illustrates the whole control structure of the conventional PSC-PWM control scheme [8] and includes two different control loops named the averaging control and the balancing control. This control structure has been chosen for

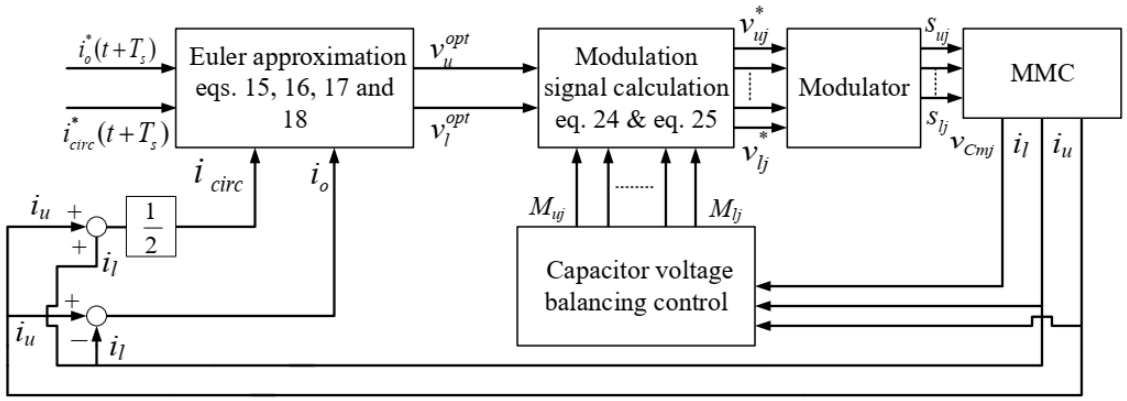

FIGURE 3. The structure of the proposed scheme.

the comparison with the proposed method because of realization in a single and three-phase converter system. Additionally, this is a representative cascaded control method using PI controllers.

1) THE AVERAGING CONTROL LOOP

Here, the difference between the nominal capacitor voltage v_C^* and the average capacitor voltage $\bar{v_C}$ is used to generate a circulating current reference through the first PI controller.

$$\bar{v_C} = \frac{1}{2N}\left(\sum_{j=1}^{N} v_{Cuj} + \sum_{j=1}^{N} v_{Clj}\right) \tag{7}$$

where v_{Cuj} and v_{Clj} $(j = 1 \sim N)$ are SM voltages of upper and lower arms, respectively.

After that, a voltage reference v_A^* is obtained through the second PI controller based on the differential value between the measured circulating current i_{circ} and its reference i_{circ}^*. The voltage reference v_A^* can be described as

$$v_A^* = K_3\left(i_{circ} - i_{circ}^*\right) + K_4 \int \left(i_{circ} - i_{circ}^*\right) dt, \tag{8}$$

where

$$i_{circ}^* = K_1\left(v_C^* - \bar{v_C}\right) + K_2 \int \left(v_C^* - \bar{v_C}\right) dt. \tag{9}$$

2) THE BALANCING CONTROL LOOP

The balancing control loop guarantees the balancing of the capacitor voltage among all SMs of the MMC. A P-controller carries out this task by generating output from the difference between the nominal capacitor voltage v_C^* and each capacitor voltage v_{Cmj} $(m = u, l)$. This output is multiplied by 1 or -1 based on the signs of the arm currents (Figure 2) to generate individual voltage references v_{Bmj}^* that are added to the voltage reference of each SM. Hence, the pulse width of the corresponding SM is adjusted to balance the capacitor voltage:

$$v_{Bmj}^* = \pm K_5\left(v_C^* - v_{Cmj}\right). \tag{10}$$

The arm reference modulating signals can be obtained by combining (8) and (10):

$$v_{uj}^* = v_A^* + v_{Buj}^* - \frac{v_o^*}{N} + \frac{V_{dc}}{2N}, \tag{11}$$

$$v_{lj}^* = v_A^* + v_{Blj}^* + \frac{v_o^*}{N} + \frac{V_{dc}}{2N}, \tag{12}$$

where v_o^* is an AC voltage reference. The PWM signal of each SM is generated by comparing the arm reference modulating signals with the associated triangular carriers that are phase-shifted by $2\pi/(2N)$ to achieve harmonic cancellation.

Apparently, the conventional PSC-PWM control scheme based on PI controllers requires great effort to tune and design the PI parameters, which exerts a negative impact to converter operation performance if PI parameters are not selected properly. In addition, the utilization of different PI controllers to achieve the control objectives reduces the dynamic performance [24].

III. THE PROPOSED SCHEME

The proposed method is divided into two main parts: an arm voltage reference modulating signal generation and a voltage balancing control, as depicted in Figure 3. Based on the mathematical model presented in Section II, the arm voltage reference modulating signals are generated using the predicted values for the AC output current and the circulating current. Meanwhile, the capacitor voltage balancing control task is carried out by rescaling the modulation indexes of each SM reference modulation signal. Unlike the conventional PSC-PWM control scheme method based on PI controllers [8], the proposed method is easy to realize with a straightforward approach because the PI parameters tuning procedure is unnecessary, thus permitting a significantly improved dynamic performance.

A. THE PREDICTED ARM VOLTAGE REFERENCE MODULATING SIGNALS

From (5) and (6), we can conclude that the AC output current can be controlled by the difference between v_u and v_l, while the circulating current is controlled by the sum of v_u and v_l.

The discrete-time model of the AC output current and circulating current can be obtained using the Euler approximation [23] as

$$i_o\left(t+T_s\right)=\left(\frac{T_s}{2L+L_a}\right)\left[v_l\left(t\right)-v_u(t)\right]+\left(1-\frac{2RT_s}{2L+L_a}\right)i_o\left(t\right), \tag{13}$$

$$i_{circ}\left(t+T_s\right)=\left(\frac{T_s}{2L_a}\right)\left[V_{dc}-v_l\left(t\right)-v_u(t)\right]+i_{circ}\left(t\right). \tag{14}$$

From (13) and (14), the upper and lower arm voltages can be calculated following the measured and predicted value of the AC output current and the circulating current as

$$v_u\left(t\right)=\frac{V_{dc}}{2}-\frac{2L+L_a}{2T_s}\left[i_o\left(t+T_s\right)-i_o\left(t\right)\right]-Ri_o\left(t\right)-\frac{L}{T_s}\left[i_{circ}\left(t+T_s\right)-i_{circ}\left(t\right)\right] \tag{15}$$

$$v_l\left(t\right)=\frac{V_{dc}}{2}+\frac{2L+L_a}{2T_s}\left[i_o\left(t+T_s\right)-i_o\left(t\right)\right]+Ri_o\left(t\right)-\frac{L}{T_s}\left[i_{circ}\left(t+T_s\right)-i_{circ}\left(t\right)\right] \tag{16}$$

The aim of the AC output current and the circulating current control is to regulate them following their references. Therefore, from (15) and (16), the predicted AC output current $i_o\left(t+T_s\right)$ and the predicted circulating current $i_{circ}\left(t+T_s\right)$ can be replaced by their respective reference values $i_o^*(t+T_s)$ and $i_{circ}^*(t+T_s)$ to calculate the ideal upper and lower arm voltages. Hence, the optimal upper arm and lower arm voltages are given as

$$v_u^{opt}=\frac{V_{dc}}{2}-\frac{A+B}{2}, \tag{17}$$

$$v_l^{opt}=\frac{V_{dc}}{2}+\frac{A-B}{2}, \tag{18}$$

where

$$A=\frac{2L+L_a}{T_s}\left[i_o^*\left(t+T_s\right)-i_o\left(t\right)\right]+2Ri_o\left(t\right) \tag{19}$$

and

$$B=\frac{2L}{T_s}\left[i_{circ}^*(t+T_s)-i_{circ}(t)\right]. \tag{20}$$

The reference for the circulating current is calculated based on the real power transferred to the dc side by

$$I_{dc}^*=-\frac{P}{V_{dc}}, \tag{21}$$

whereas $i_{circ}^*=I_{dc}^*$ for one-phase MMC system and $i_{circ}^*=\frac{I_{dc}^*}{3}$ for three-phase MMC system [22].

B. VOLTAGE BALANCING CONTROL

In the PSC-PWM, each carrier corresponds to the switching state of a single SM. The difference between each SM means that an imbalance can occur in the capacitor voltage among the SM capacitors. The capacitor voltage balancing task is usually carried out by adding a term that depends on the capacitor voltage error and either the arm current [8] or the circulating current [10] to each SM's modulation signal. However, this scheme cannot avoid the PI parameters tuning procedure and would produce low-order harmonics in the output voltage due to the negative effect from the component of sign of the arm current as in (10). Therefore, we propose a capacitor voltage balancing control scheme by rescaling the modulation indexes of the reference modulating signals. The proposed scheme eliminates both the requirement of the PI parameters tuning procedure and unwanted switching actions like the capacitor voltage sorting algorithm.

In addition to the reason for the imbalance among the SM capacitor voltages mentioned previously, there are cases in which all the SMs on one arm in an MMC are inserted for a time period that causes them to charge or discharge excessively. This can accumulate and enlarge the imbalance of capacitor voltages in MMCs, which negatively impacts their operation. To solve these problems, the proposed capacitor voltage balancing control scheme rescales the modulation indexes of each SM reference modulation signal following the relationship between the instantaneous value of the capacitor voltage and the direction of the arm current to manage the amount of power present in each SM of the MMC. A coefficient is calculated by the division between the capacitor voltage of each SM v_{Cj} and the average capacitor $\overline{v_C}$voltage, which is presented as

$$M_{uj}=\frac{v_{Cuj}}{\overline{v_C}}, \tag{22}$$

$$M_{lj}=\frac{v_{Clj}}{\overline{v_C}}. \tag{23}$$

The calculated coefficients M_{mj} can be assigned to the reference modulating signal of each SM to rescale the modulation indexes and thus satisfy the charge balance. If the arm current is positive, a high M_{mj} is assigned to the SM modulating signal of the corresponding low capacitor voltage to charge more, and a low M_{mj} is assigned to the SM modulating signal of the corresponding high capacitor voltage to charge less. Meanwhile, if the arm current is negative, a high M_{mj} is assigned to the SM modulating signals of the corresponding high capacitor voltage to discharge more, and vice versa. This scheme lets us balance the capacitor voltage and prevents excessive voltage charging or discharging in MMCs.

The capacitor voltage balancing control scheme shown in Figure 4 is proposed based on previous analysis. In the proposed control scheme, the capacitor voltages are sorted into ascending order if the arm currents are positive. Meanwhile, coefficients M_j are calculated by (21), (22) and sorted into descending order. Next, the highest coefficients M_j are assigned to the reference modulating signal of the lowest

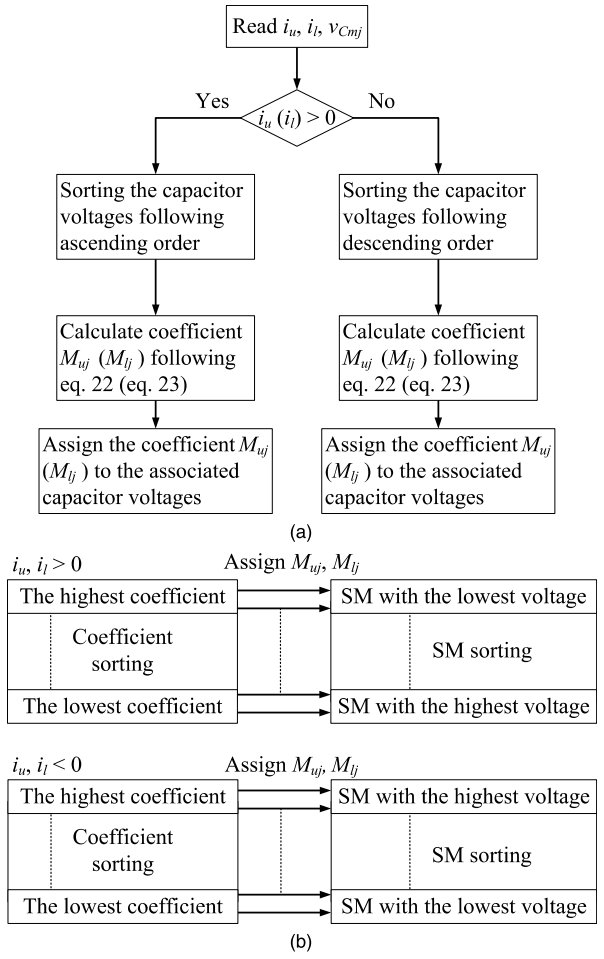

FIGURE 4. The structure of the proposed capacitor voltage balancing control: (a) a block diagram of the whole structure and (b) the coefficient assigning procedure.

capacitor voltage. This procedure is executed sequentially from the highest coefficient M_j to the lowest one. In contrast, if the arm currents are negative, the capacitor voltages and calculated coefficients $M_j$are sorted into descending order. The highest coefficient M_j is assigned to the reference modulating signal of the highest capacitor voltage and then continually assigned until reaching the lowest capacitor voltage.

Finally, the arm reference modulating signals of each SM are yielded by assigning the associated coefficient using the following equations:

$$v_{uj}^{*} = \frac{V_{dc}}{2} - M_{uj} \times \frac{A+B}{2}, \tag{24}$$

$$v_{lj}^{*} = \frac{V_{dc}}{2} + M_{lj} \times \frac{A-B}{2}. \tag{25}$$

Similar to the PSC-PWM method, the arm reference modulating signals are compared with the corresponding triangle carriers to generate PWM signals. Figure 3 illustrates the proposed scheme's whole structure. In addition, it is apparent that the whole control structure does not require any PI controllers, which makes the greatly time-consuming PI parameters tuning procedure as per the conventional method unnecessary and dependence of converter operation performance on PI adjustment. This allows the easy realization of the proposed scheme.

TABLE 2. Parameters of the single-phase MMC for simulation.

DC-link voltage V_{dc} (V)	7000
SMs per arm N	3
SM capacitor voltage V_C (V)	2333,3
SM capacitance C (μF)	3000
Arm inductance L_a (mH)	4
Load inductance L (mH)	10
Load resistance R (Ω)	20
Output frequency f_o (Hz)	60
Carrier frequency f_c (kHz)	2
Rated MMC kVA S (kVA)	700
Sampling frequency f_{sp} (kHz)	10

TABLE 3. Controller parameters.

Parameter	Value
K_1	0.5
K_2	10
K_3	1
K_4	10
K_5	0.4

IV. SIMULATION AND EXPERIMENTAL RESULTS

A. SIMULATION RESULTS

To verify the proposed method's performance, the simulation of a single-phase MMC with $N = 3$ was implemented using PSIM software, the system parameters for which are given in Table 2. The PI parameters used in this comparison are shown in Table 3, which are selected by using a trial and error method. The PI parameters are selected in order to give the operation performance as good as possible. This ensures a fair comparison with the proposed method.

Figure 5 illustrates the steady-state performance of the proposed method and the conventional method over a total simulation time of 0.1 s. As depicted, there was no noticeable difference in the AC output current between the two methods. The AC output current of the proposed method showed the same quality as that of the conventional method with a good sinusoidal form and THD = 0.38%. With $N = 3$ SMs per arm, both control methods generated a seven-level output voltage that varied in the range $-V_{dc}/2$ to $V_{dc}/2$. The capacitor voltages remained balanced at the nominal value of 2.3 kV ($V_{dc}/3$) in both methods. However, in terms of the circulating current, the proposed scheme showed a better result than the conventional method. The second-harmonic circulating current is evident in Figure 5(b) due to the circulating current being regulated through the sum of capacitor voltages (Figure 2), so it cannot be directly manipulated. Although the circulating current with this conventional scheme can be suppressed further by using some sort of extra controller

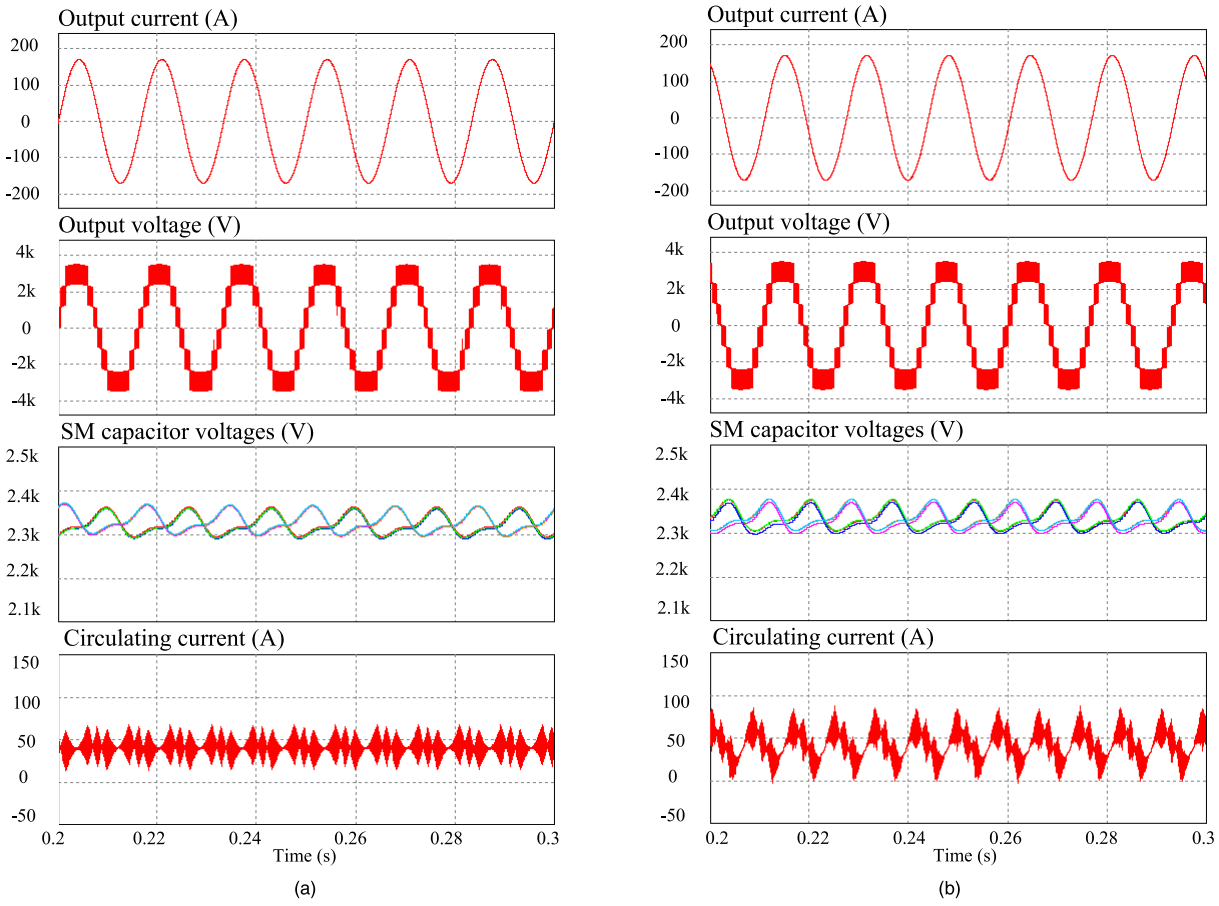

FIGURE 5. Simulated waveforms of the AC output current, output voltage, SM capacitor voltages, and circulating current obtained by a seven-level MMC ($N = 3$) during steady-state operation by (a) the proposed method and (b) the conventional method.

(PI, PR, repetitive, etc.) as mentioned in the Introduction section, this significantly increases the complexity of the control method and the designing and tuning controller procedure. By eliminating the second-harmonic circulating current, the proposed method allows a reduced power loss (by the reduction of the RMS arm current [29]) that is better than the conventional method. Figure 6(a) and 6(b) show the simulation waveforms for the FFT analysis of the circulating current in the steady-state from each method. Hence, the simulation waveform results verify the proposed method's proper operation and high stability.

Figure 7(a) and 7(b) illustrate the dynamic-response performance of the proposed method and the conventional method, respectively. The MMC was initially controlled to supply a current of 170 A to the load. At t = 0.25 s, the magnitude of the AC output current reference was decreased from 170 to 85 A. The output currents of both control concepts correctly tracked the sinusoidal form and magnitude. The output voltage level was reduced from 7 to 5 V, and the capacitor voltages remained at the nominal value with smaller oscillations. In this case, the proposed method achieved a stable state faster than the conventional method since it does not use various PI controllers to control the capacitor voltage balancing. Regarding the circulating current, the reduction in the AC output current reference resulted in a decrease in the arm currents. Thus the magnitude of the circulating current also decreased

The simulation waveform results during dynamic-response operation validated the proper operation and correct algorithm of the proposed method; furthermore, the better dynamic performance of the proposed method compared with the conventional method was verified.

B. EXPERIMENTAL RESULTS

The proposed method was evaluated by conducting an experiment on a single-phase MMC laboratory prototype. The MMC laboratory prototype configuration and photographs are presented in Figure 8(a) and 8(b), respectively. The single-phase MMC laboratory prototype contains three half-bridge SMs in each arm that generates seven levels of output voltage ($N = 3$). The proposed method and conventional method were implemented for performance comparison purpose, and both of them are realized through a Texas Instruments TMS320F28335 digital signal processor (DSP); Table 4 presents the circuit parameters. Figure 9 shows the digital control system used for the experiment. The system

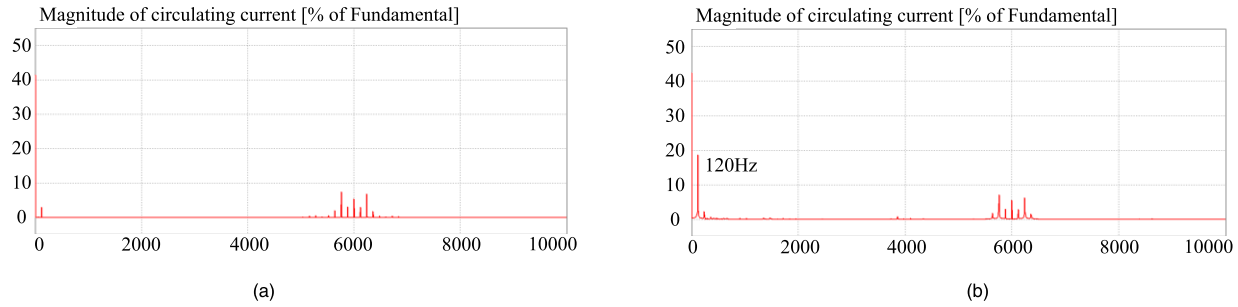

FIGURE 6. Simulated waveforms of the fast Fourier transform (FFT) analysis of the circulating current at steady-state operation by (a) the proposed method and (b) the conventional method.

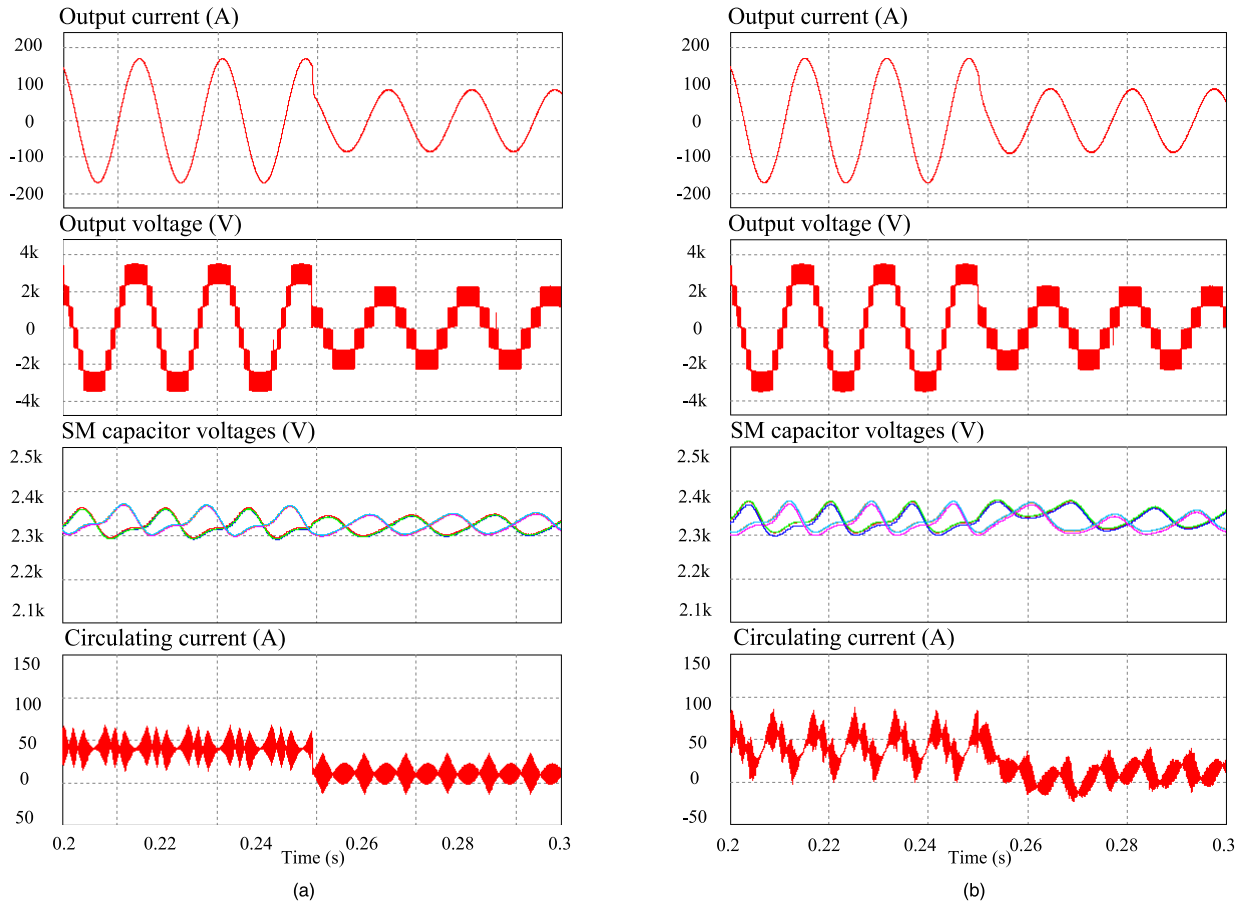

FIGURE 7. Simulated waveforms of the AC output current, output voltage, SM capacitor voltages, and circulating current obtained by a seven-level MMC ($N = 3$) during dynamic-response operation by (a) the proposed method and (b) the conventional method.

detects the SM capacitor voltage v_{Cmj} and the upper and lower arm current i_u, and i_l through voltage sensors and current sensors, respectively. The capacitor voltages are monitored in real-time and sampled at the sampling frequency $f_{sp} = 5$kHz. The control algorithm is executed by DSP, which generates the switching states transmitted to the MMC.

Figure 10 shows the experimental waveforms during steady-state operation by the proposed method and the conventional method. As can be seen, both control methods generated correct sinusoidal waveforms for the AC output current with low THD values of 1.27% and 1.31% for the proposed method and the conventional method, respectively. The output voltage waveforms contain sufficient seven-level variance from $-V_{dc}/2$ to $V_{dc}/2$. The waveforms of the capacitors v_{Cu1} and v_{Cl1} show that the capacitor voltages were well balanced at 66.666 V. The circulating current synthesized by the conventional method was suppressed but still contained the second-harmonic component, as was seen in the simulation study. Meanwhile, the proposed method eliminated the second-harmonic component and suppressed the circulating

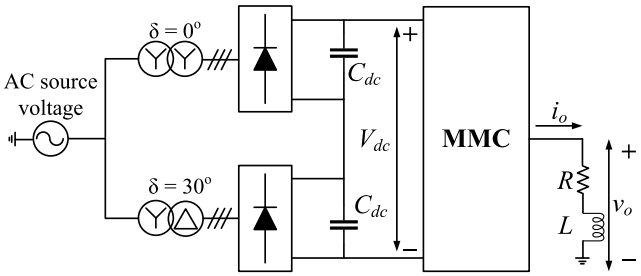

(a)

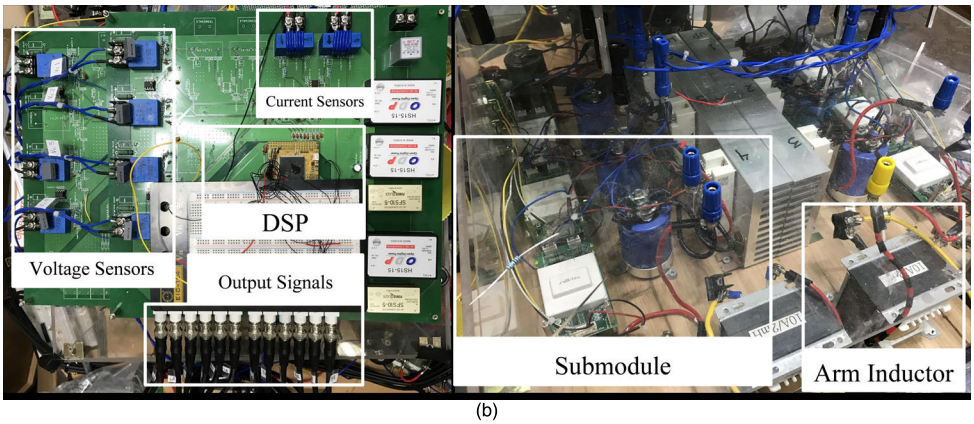

(b)

FIGURE 8. The experimental setup of the single-phase seven-level MMC: (a) a circuit diagram and (b) the single-phase seven-level prototype and control board.

TABLE 4. Experimental parameters of the single-phase MMC.

DC-link voltage V_{dc} (V)	200
SMs per arm N	3
SM capacitor voltage V_C (V)	66.666
SM capacitance C (μF)	2200
Arm inductance L_a (mH)	4
Load inductance L (mH)	10
Load resistance R (Ω)	20
Output frequency f_o (Hz)	60
Carrier frequency f_c (kHz)	2
Rated MMC kVA S (kVA)	0.2
Sampling frequency f_{sp} (kHz)	5

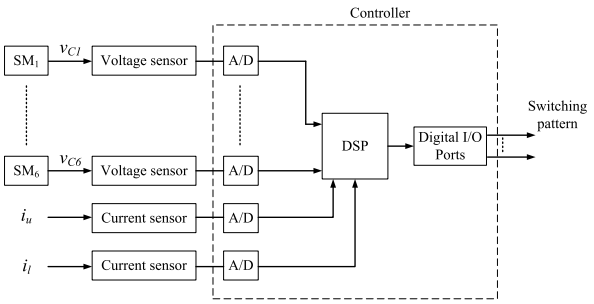

FIGURE 9. Digital control system used for the experiment.

current well. The high stability of the experimental results verifies the proposed method's correction and performance.

Figure 11 illustrates the dynamic performance of the proposed method and the conventional method with a step-change in the peak output current from 2 to 4 A. Evidently, the output current in Figure 11(a) changed very rapidly to the new reference value without overshooting. Furthermore, the output voltage waveforms yielded from both control concepts increased from five levels to seven, which corresponds to a step-change in the reference AC output current. The increased oscillation of the capacitor voltages and the increased magnitude of the circulating current by the methods (Figure 11(a) and 11(b)) were achieved properly following the change in the AC output current reference. Under dynamic-response conditions, the proposed method continued operating well, which clearly validates the proposed method's high performance.

Figure 12 shows the magnification of the AC output current and the output voltage dynamic waveforms to compare the dynamic-response performance between the proposed and conventional methods. Figure 12(a) and 12(b) depict the dynamic response when applying the proposed and conventional methods, respectively. Evidently, the AC output current from both control concepts tracked the reference correctly. However, the dynamics in the AC output current from the proposed method was higher than the conventional method. The conventional method requires around 3 ms to reach stability while the proposed method only needed approximately 1.5 ms to totally change state. This is because the conventional method is limited by the calculation time for the

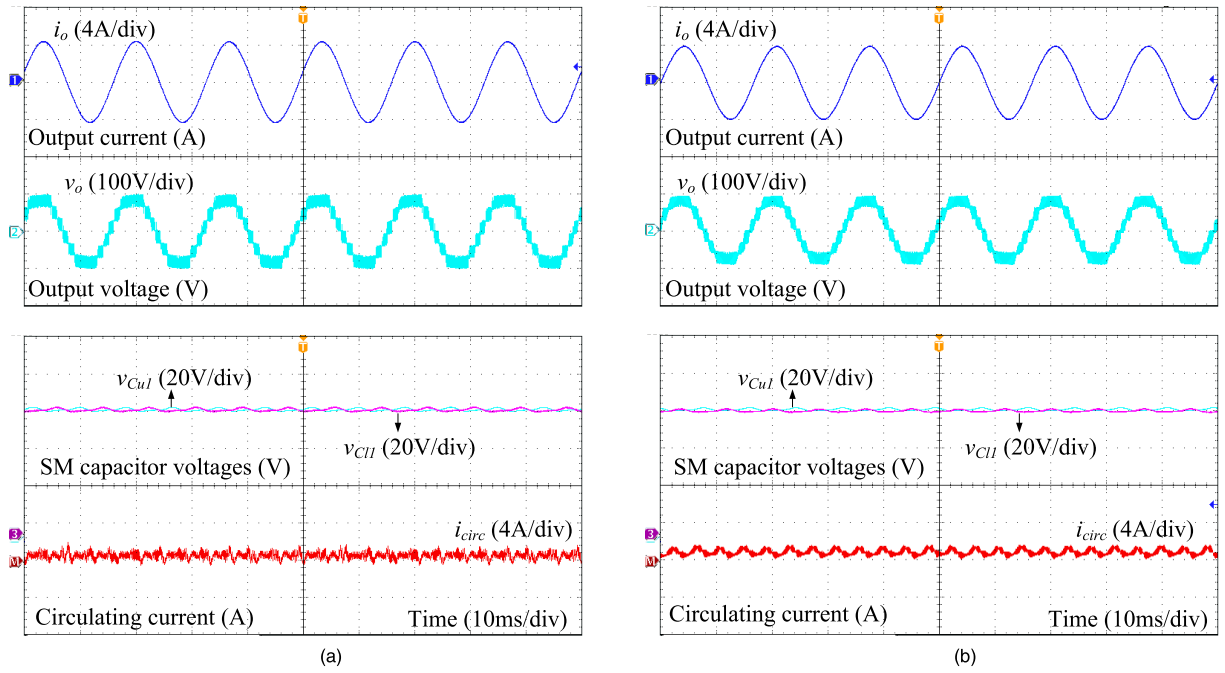

FIGURE 10. Experimental waveforms of the AC output current, output voltage, SM capacitor voltages, and circulating current obtained by the seven-level MMC ($N = 3$) during steady-state operation by (a) the proposed method and (b) the conventional method.

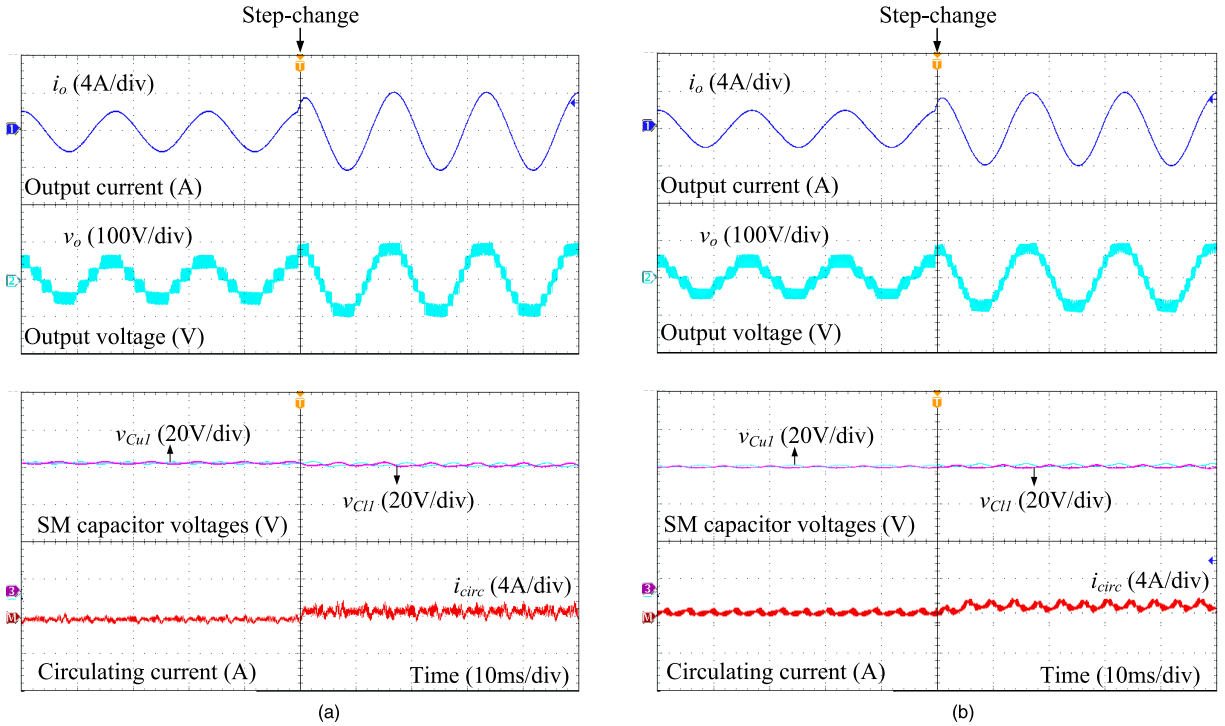

FIGURE 11. Experimental waveforms of the AC output current, output voltage, SM capacitor voltages, and circulating current obtained by the seven-level MMC ($N = 3$) during dynamic-response operation with the AC output current reference from 2A to 4A (a) the proposed method and (b) the conventional method.

reference values from the various PI controllers for the control objectives, whereas the proposed method does not require any PI controllers. This indicates the proposed method's high dynamic performance. Hence, the experimental results apparently prove the proposed method's proper operation and high dynamic performance.

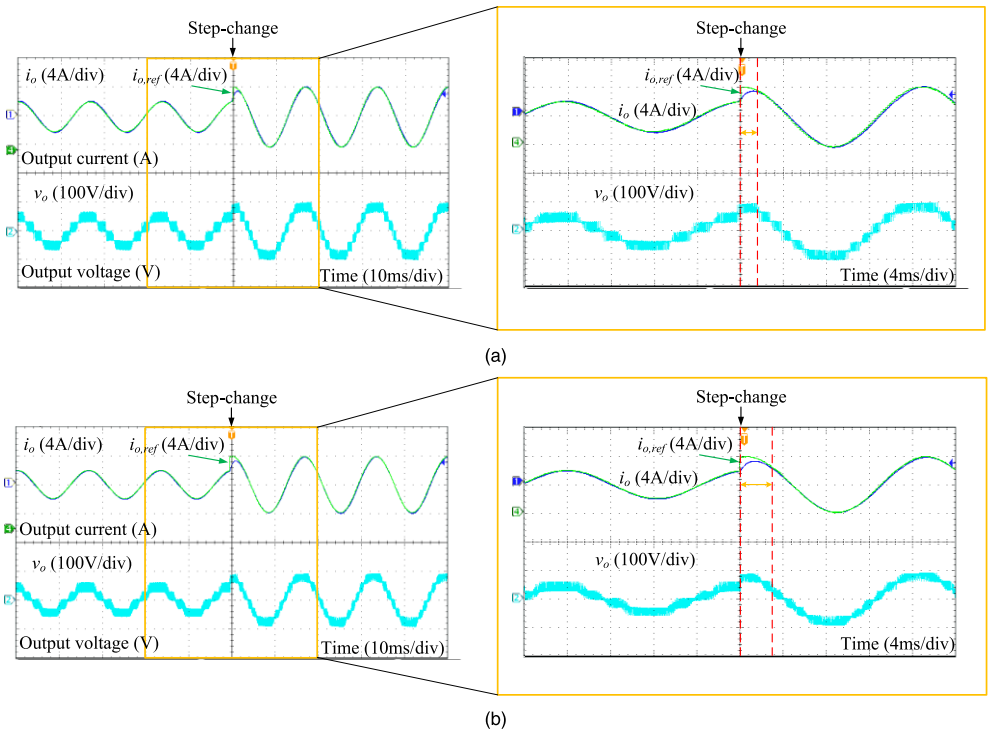

FIGURE 12. Magnified experimental waveforms of the AC output current and output voltage obtained by the seven-level MMC ($N = 3$) during dynamic-response operation by (a) the proposed method and (b) the conventional method.

V. CONCLUSION

In this paper, we present a method for the control of MMC where the proposed improved PSC-PWM and the capacitor voltage balancing control method not only inherit the merits of both the classical control and MPC methods but also have distinctive features. Using the predicted output current and circulating current and the relationship corresponding to the arm voltage, the arm reference modulating signals are generated without requiring PI or PR controllers, which eliminates the tedious PI parameter tuning procedure and dependence of converter operation performance on PI parameters adjustment. Furthermore, the balance of the SM capacitor voltages is addressed by assigning a proper coefficient generated by the relationship between the arm currents and the instantaneous values of the capacitor voltages to the associated reference modulating signal of each SM to rescale the modulation indexes. The proposed control method was compared with the conventional PSC-PWM method based on PI controllers under both simulated and experimental conditions. The two control concepts achieved good results for the control objectives and stable operation during both steady-state and dynamic-response operations. However, the proposed method had significantly improved dynamic performance compared with the classical control method, as shown by the experimental results. The correction and high performance of the proposed method are apparent and verified.

REFERENCES

[1] J. Rodriguez, S. Bernet, P. K. Steimer, and I. E. Lizama, "A survey on neutral-point-clamped inverters," *IEEE Trans. Ind. Electron.*, vol. 57, no. 7, pp. 2219–2230, Jul. 2010.

[2] S. Kouro, M. Malinowski, K. Gopakumar, J. Pou, L. G. Franquelo, B. Wu, J. Rodriguez, M. A. Pérez, and J. I. Leon, "Recent advances and industrial applications of multilevel converters," *IEEE Trans. Ind. Electron.*, vol. 57, no. 8, pp. 2553–2580, Aug. 2010.

[3] M. Malinowski, K. Gopakumar, J. Rodríguez, and M. A. Pérez, "A survey on cascaded multilevel inverters," *IEEE Trans. Ind. Electron.*, vol. 57, no. 7, pp. 2197–2206, Jul. 2010.

[4] S. S. Fazel, S. Bernet, D. Krug, and K. Jalili, "Design and comparison of 4-kV neutral-point-clamped, flying-capacitor, and series-connected h-bridge multilevel converters," *IEEE Trans. Ind. Appl.*, vol. 43, no. 4, pp. 1032–1040, Jul./Aug. 2007.

[5] J. Pou, R. Pindado, and D. Boroyevich, "Voltage-balance limits in four-level diode-clamped converters with passive front ends," *IEEE Trans. Ind. Electron.*, vol. 52, no. 1, pp. 190–196, Feb. 2005.

[6] A. Lesnicar and R. Marquardt, "An innovative modular multilevel converter topology suitable for a wide power range," in *Proc. IEEE Bologna Power Tech Conf.*, Bologna, Italy, Jun. 2003, p. 6.

[7] S. Debnath, J. Qin, B. Bahrani, M. Saeedifard, and P. Barbosa, "Operation, control, and applications of the modular multilevel converter: A review," *IEEE Trans. Power Electron.*, vol. 30, no. 1, pp. 37–53, Jan. 2015.

[8] M. Hagiwara and H. Akagi, "Control and experiment of pulsewidth-modulated modular multilevel converters," *IEEE Trans. Power Electron.*, vol. 24, no. 7, pp. 1737–1746, Jul. 2009.

[9] M. Vasiladiotis, N. Cherix, and A. Rufer, "Accurate capacitor voltage ripple estimation and current control considerations for grid-connected modular multilevel converters," *IEEE Trans. Power Electron.*, vol. 29, no. 9, pp. 4568–4579, Sep. 2014.

[10] R. Lizana, C. Castillo, M. A. Perez, and J. Rodriguez, "Capacitor voltage balance of MMC converters in bidirectional power flow operation," in *Proc. 38th Annu. Conf. IEEE Ind. Electron. Soc. (IECON)*, Montreal, QC, Canada, Oct. 2012, pp. 4935–4940.

[11] Q. Tu, Z. Xu, and L. Xu, "Reduced switching-frequency modulation and circulating current suppression for modular multilevel converters," *IEEE Trans. Power Del.*, vol. 26, no. 3, pp. 2009–2017, Jul. 2011.
[12] B. Chen, Y. Chen, C. Tian, J. Yuan, and X. Yao, "Analysis and suppression of circulating harmonic currents in a modular multilevel converter considering the impact of dead time," *IEEE Trans. Power Electron.*, vol. 30, no. 7, pp. 3542–3552, Jul. 2015.
[13] S. Li, X. Wang, Z. Yao, T. Li, and Z. Peng, "Circulating current suppressing strategy for MMC-HVDC based on nonideal proportional resonant controllers under unbalanced grid conditions," *IEEE Trans. Power Electron.*, vol. 30, no. 1, pp. 387–397, Jan. 2015.
[14] L. He, K. Zhang, J. Xiong, and S. Fan, "A repetitive control scheme for harmonic suppression of circulating current in modular multilevel converters," *IEEE Trans. Power Electron.*, vol. 30, no. 1, pp. 471–481, Jan. 2015.
[15] M. Zhang, L. Huang, W. Yao, and Z. Lu, "Circulating harmonic current elimination of a CPS-PWM-based modular multilevel converter with a plug-in repetitive controller," *IEEE Trans. Power Electron.*, vol. 29, no. 4, pp. 2083–2097, Apr. 2014.
[16] S. Fan, K. Zhang, J. Xiong, and Y. Xue, "An improved control system for modular multilevel converters with new modulation strategy and voltage balancing control," *IEEE Trans. Power Electron.*, vol. 30, no. 1, pp. 358–371, Jan. 2015.
[17] R. Darus, J. Pou, G. Konstantinou, S. Ceballos, and V. G. Agelidis, "Circulating current control and evaluation of carrier dispositions in modular multilevel converters," in *Proc. IEEE ECCE Asia Downunder*, Melbourne, VIC, Australia, Jun. 2013, pp. 332–338.
[18] R. Naderi and A. Rahmati, "Phase-shifted carrier PWM technique for general cascaded inverters," *IEEE Trans. Power Electron.*, vol. 23, no. 3, pp. 1257–1269, May 2008.
[19] J. Rodríguez, J. Pontt, C. A. Silva, P. Correa, P. Lezana, P. Cortes, and U. Ammann, "Predictive current control of a voltage source inverter," *IEEE Trans. Ind. Electron.*, vol. 54, no. 1, pp. 495–503, Feb. 2007.
[20] S. Kouro, P. Cortes, R. Vargas, U. Ammann, and J. Rodríguez, "Model predictive control—A simple and powerful method to control power converters," *IEEE Trans. Ind. Electron.*, vol. 56, no. 6, pp. 1826–1838, Jun. 2009.
[21] J. Bocker, B. Freudenberg, A. The, and S. Dieckerhoff, "Experimental comparison of model predictive control and cascaded control of the modular multilevel converter," *IEEE Trans. Power Electron.*, vol. 30, no. 1, pp. 422–430, Jan. 2015.
[22] M. Vatani, B. Bahrani, M. Saeedifard, and M. Hovd, "Indirect finite control set model predictive control of modular multilevel converters," *IEEE Trans. Smart Grid*, vol. 6, no. 3, pp. 1520–1529, May 2015.
[23] Z. Gong, P. Dai, X. Yuan, X. Wu, and G. Guo, "Design and experimental evaluation of fast model predictive control for modular multilevel converters," *IEEE Trans. Ind. Electron.*, vol. 63, no. 6, pp. 3845–3856, Jun. 2016.
[24] B. Gutierrez and S.-S. Kwak, "Modular multilevel converters (MMCs) controlled by model predictive control with reduced calculation burden," *IEEE Trans. Power Electron.*, vol. 33, no. 11, pp. 9176–9187, Nov. 2018.
[25] M. H. Nguyen and S. Kwak, "Simplified indirect model predictive control method for a modular multilevel converter," *IEEE Access*, vol. 6, pp. 62405–62418, 2018.
[26] M. Hiller, D. Krug, R. Sommer, and S. Rohner, "A new highly modular medium voltage converter topology for industrial drive applications," in *Proc. 13th Eur. Conf. Power Electron. Appl.*, Barcelona, Spain, Sep. 2009, pp. 1–10.
[27] S. Rohner, S. Bernet, M. Hiller, and R. Sommer, "Modulation, losses, and semiconductor requirements of modular multilevel converters," *IEEE Trans. Ind. Electron.*, vol. 57, no. 8, pp. 2633–2642, Aug. 2010.
[28] A. Dekka, B. Wu, R. L. Fuentes, M. Perez, and N. R. Zargari, "Evolution of topologies, modeling, control schemes, and applications of modular multilevel converters," *IEEE J. Emerg. Sel. Topics Power Electron.*, vol. 5, no. 4, pp. 1631–1656, Dec. 2017.
[29] X. Li, Q. Song, W. Liu, S. Xu, Z. Zhu, and X. Li, "Performance analysis and optimization of circulating current control for modular multilevel converter," *IEEE Trans. Ind. Electron.*, vol. 63, no. 2, pp. 716–727, Feb. 2016.

MINH HOANG NGUYEN received the B.S. degree in electrical and electronics engineering from the Hanoi University of Science and Technology, Vietnam, in 2016. He is currently pursuing the M.S. and Ph.D. combined degrees in electrical and electronics engineering with Chung-Ang University, Seoul, South Korea. His research interest is control for multilevel converters.

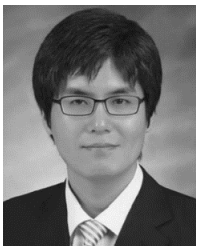

SANGSHIN KWAK (S'02–M'05) received the Ph.D. degree in electrical engineering from Texas A&M University, College Station, TX, USA, in 2005. From 2007 to 2010, he was an Assistant Professor with Daegu University, Gyeongsan, South Korea. Since 2010, he has been with Chung-Ang University, Seoul, South Korea, where he is currently a Professor. His research interests are topology design, modeling, control, and analysis of ac/dc, dc/ac, and ac/ac power converters, including resonant converters for adjustable-speed drives and digital display drivers, and modern control theory applied to digital-signal-processing-based power electronics.

TAEHYUNG KIM (S'00–M'04–SM'12) received the Ph.D. degree from Texas A&M University, College Station, TX, USA, in 2003.

In 2005, he joined the Department of Electrical and Computer Engineering, University of Michigan–Dearborn, Dearborn, MI, USA, where he is currently an Associate Professor. In 2014, he visited Chung-Ang University as an Invited Brain Pool Research Scholar. Dr. Kim received the 2012 Second Prize Paper Award from the IEEE Industry Applications Society (Annual Society's Best Magazine Article).